IJME

Int. J. of Applied Mechanics and Engineering, 2023, vol.28, No.2, pp.90-112
DOI: 10.59441/ijame/168933

AN UNSTEADY ELECTRO-MAGNETOHYDRODYNAMIC TWO-LIQUID PLASMA FLOW ALONG A CHANNEL OF INSULATING POROUS PLATES WITH HALL CURRENTS

V.Gowri Sankara Rao
Dept. of Mathematics, St. Joseph's College for Women (A), Visakhapatnam, Pin code: 530004, A.P., INDIA

T. Linga Raju*
Department of Engineering Mathematics, AUCE(A),
Andhra University, Visakhapatnam,Pin code: 530003 A.P., INDIA
E-mail: tlraju45@yahoo.com

It is proposed to use the Hall currents to model the transient magneto-hydrodynamic two liquid flows and heat transfer of ionized gases propelled by a common pressure gradient via a horizontal channel consisting of parallel porous plates. For the distributions of velocity and temperature, the principal partial differential equations that explain heat transfer flow under the chosen constraints are resolved. Graphical representations are given for the distributions of velocity, temperature, and heat transfer rates. This research will be carried out using non-conducting porous plate's channel.

Key words: Hall effect, MHD heat transfer, plasma, immiscible flow, non conducting porous plates.

1. Introduction

In the decades-long research there has been a progressively impressive enthusiasm for investigating electro-magnetohydrodynamic (EMHD) two-fluid flow through channels, pipes or tubes. The transient phenomenon of such flows has been the subject of numerous research studies [1-5]. A few examples of applications in engineering and technology as well as industry-related different energy transformation frameworks that have sparked interest in this area include the development of conceptual designs for fluid metal magneto-hydrodynamic (MHD) power generators, accelerators, and fusion reactors. These applications therefore demand in-depth and reliable understanding of thermo-hydraulic systems with two-phase/two-fluid flow with an externally applied magnetic field. Two-fluid/ two-phase flows are also encountered in the petrochemical industry during the transportation and extraction of oil.

There are many astronomical and geophysical problems, such as plasma streams in an MHD control generator, radio propagation through ionized gases, plasma jets, as well as Hall accelerators, which depend greatly on Hall currents. While the magnetic field strength is extremely strong with a low density fluid, the Hall impact cannot be ignored because it affects how plasma flows differently. Many researchers, including Cowling [6], Sherman and Sutton [7], Sato [8], Shercliff [9], Raju and Rao [10], Ram [11], and many more authors, have conducted model examinations on the impact of Hall-currents on EMHD flows. Sakhnovskii [12], Jana and Datta [13], Beg *et al.* [14] and many have studied these consequences for the unsteady situation. Additionally, it is believed in the literature that the existence of hydro-magnetic forces and Hall currents has had a significant impact on the MHD flow behavior in channel flows with porous boundaries. As a result of their use in many engineering and technological fields, numerous studies have been accounted for in the literature.Among these, the works of Rama Bhargava and Meena Rani [15], Raju and Rao [16],

* To whom correspondence should be addressed

Ganesh and Krishnambal [17], Ghosh *et al.* [18], Gupta *et al.* [19], Khaled [20] and many more are worth mentioning.

Numerous researchers have explored the MHD heat transfer in two-fluid/or two-phase flows under a few specific circumstances without taking the Hall effects into account. In Lohrasbi and Sahai's [21] investigation of MHD two-phase stream with temperature-dependent transport characteristics, they dealt with a numerical approach to the problem of heat transfer caused by the MHD Poiseuille flow of two incommensurable fluids in a straight channel. A problem of MHD two-fluid heat flow for a short circuit model was studied by Malashetty and Leela in [22]. They thought about a similar issue for the open circuit case [23]. The unstable MHD convective heat and mass transfer via a semi-boundless vertical permeable moving plate with heat transfer was investigated by Chamkha [24]. Sharma and Rani [25] looked into the effects of compressibility and a finite Larmor radius on the thermosolutal instability of plasma. The Hall effects on the thermosolutal instability of plasma were examined by Sharma and Rani in [26]. Zivojin *et al.* [27] investigated the heat transfer and magnetohydrodynamic flow of two incommensurable fluids with induced magneticfield effects. Abdul [28] thought of the momentary magnetohydrodynamic movement of 2-incompatible fluids along a flat conduit. Heat transmission in two-ionized fluids in a horizontal conduit with an applied transverse magnetic field and Hall effect was examined by L.Raju [29]. The unsteady MHD flow of two immiscible liquids over a horizontal channel with chemical reaction was investigated by Sivakamini and Govindarajan [30]. Abd Elmaboud *et al.* [31] researched into the electromagnetic flow of immiscible liquids. L.Raju [32] used Hall currents to investigate the heat transfer in a rotating system with a hydromagnetic two-fluid flow of an ionised gas between parallel walls. L.Raju and Gowri [33] examined the effect of Hall current on the unsteady MHD 2-ionised fluid heat transfer flow within a channel. The effect of Hall currents on EMHD 2-layered plasma heat transfer flow via a channel of a porous plates was studied by Nagavalli *et al*. [34]. L.Raju and Venkat [35] investigated an unsteady EMHD flow and heat transfer of two ionized liquids in a rotating system with Hall currents for the case of insulating plates.

This article examines an issue of an unsteady electro-magnetohydrodynamic flow of two liquids and the heat transfer through a horizontal channel of non-conducting porous plates in the presence of Hall currents. This speculative research could have some practical applications in a variety of distinct fields, including geophysics, aviation science, specifically in the area of streamlined warming, and issues of engineering applications, such as pivoting MHD generators, Hall accelerators, plasma jets, spacecraft, the cooling process of thermo-atomic power reactors, the challenge of boundary layer control, and so forth.

2. Formulation and mathematical analysis

We suppose an unsteady two-dimensional electro-magneto hydrodynamic two-liquid flow of ionised gases that is controlled by a common constant pressure gradient $-\frac{\partial p}{\partial x}$ in a horizontal channel that is constrained by two parallel porous plates that stretch out in the *x*- and *z*-directions with Hall currents. A steady suction v_0 is applied normally to both plates. In the *y*-direction, a constant magnetic field B_0 is applied. Since the magnetic Reynolds number is thought to be low, it is assumed that the induced magnetic field is insignificant. In the plane parallel to the channel plates, the *x*-axis is taken in the direction of a hydrodynamic pressure gradient but not in the direction of a flow. The coordinate system and physical system for the two-fluid flow model are shown in Fig.1 with the origin placed midway between the plates. The fluids in the upper and lower zones (regions), that is, $0 \le y \le h_1$ and $h_2 \le y \le 0$ are assigned as Region-I and Region-II, respectively. Two immiscible, electrically conducting, incompressible fluids with different viscosities μ_1, μ_2, densities ρ_1, ρ_2 and electrical conductivities σ_{01}, σ_{02} are present in Regions I and II. In contrast to the channel height, the channel width is supposed to be extremely enormous. Since the size of the plates is limitless, all physical quantities – aside from pressure – will depend, on y and t. The interface between two immiscible fluids is thought to be flat, stress-free, and unaffected. And for the sake of simplicity, the following hypotheses put forth by Sato [8] and L.Raju [32] are taken into consideration (i) The electric and magnetic fields are not affecting the equilibrium state of ionisation, (ii) The impact of space

charge is ignored, iii) The magnetic Reynolds number is low, and as a result neither the generated magnetic field nor the applied magnetic field are much larger than the magnetic field that is outwardly applied to the fluid. These hypotheses lead to a thorough description of the governing equations of motion and current for the two-dimensional unsteady electro- magneto hydrodynamic two-fluid flow problem.

The main equations to be solved for the issue are the equations of motion and current for an unsteady EMHD two-fluid flow of neutral fully ionised gases valid under the aforementioned suppositions. The governing equations of motion and current for an unsteady hydromagnetic two-fluid flow of neutral fully ionised gas in a horizontal channel bounded by two parallel porous plates are shortened in both fluid regions, comparable to Spitzer [36], Sato [8], Malashetty and Leela [23]. The thermal boundary conditions are acknowledged to apply to all areas of the channel plates while disregarding thermal conduction along the flow path.

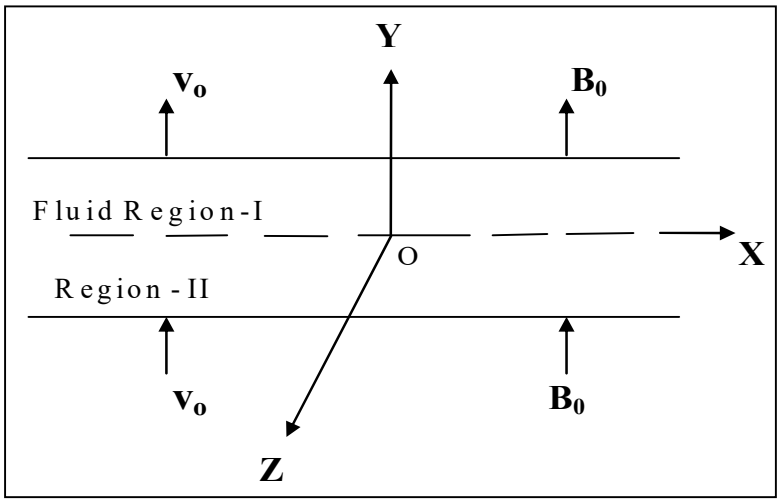

Fig.1.Flow geometry.

The equations for the research include the motion, current, and energy equations along with the boundary and interface conditions. We use the fluid's velocity as $\overline{V_i} = (u_i, 0, w_i)$, the strength of the magnetic flux as $\overline{B} = (0, B_0, 0)$, the current density as $\overline{J_i} = (J_{ix}, 0, J_{iz})$, and the electric field as $\overline{E_i} = (E_{ix}, 0, E_{iz})$ and $J_i^2 = J_{ix}^2 + J_{iz}^2, (i = 1, 2)$ for both fluid areas, according to the analysis used in the research of Sato [8] and L.Raju and Gowri [33]. As a result, the governing equations in the two fluid regions (that is, for the fluids in the upper and lower regions, i.e., Region-I and Region-II), are simplified and become as follows:

Region-I:

$$\rho_1 \frac{\partial u_1}{\partial t} = \rho_1 \nu_1 \frac{\partial^2 u_1}{\partial y^2} - \rho_1 \nu_0 \frac{\partial u_1}{\partial y} - \left\{ 1 - \left(1 - \frac{\sigma_{11}}{\sigma_{01}} \right) s \right\} \frac{\partial p}{\partial x} + \\ + \left\{ -(E_{1z} + u_1 B_0)\sigma_{11} + (E_{1x} - w_1 B_0)\sigma_{21} \right\} B_0, \tag{2.1}$$

$$\rho_1 \frac{\partial w_1}{\partial t} = \rho_1 \nu_1 \frac{\partial^2 w_1}{\partial y^2} - \rho_1 \nu_0 \frac{\partial w_1}{\partial y} + \left(s \ \frac{\sigma_{21}}{\sigma_{01}} \right) \frac{\partial p}{\partial x} + \\ + \left\{ \sigma_{11}(E_{1x} - w_1 B_0) + \sigma_{21}(E_{1z} + u_1 B_0) \right\} B_0, \tag{2.2}$$

$$\rho_1 c_{p1}\frac{\partial T_1}{\partial t} = \frac{c_{p1}\mu_1}{P_r}\frac{\partial^2 T_1}{\partial y^2} + \rho_1 v_0\frac{\partial T_1}{\partial y} + \mu_1\left[\left(\frac{\partial u_1}{\partial y}\right)^2 + \left(\frac{\partial w_1}{\partial y}\right)^2\right] + \frac{J_1^2}{\sigma_{01}}, \tag{2.3}$$

$$J_{1x} = \sigma_{11}E_{1x} - B_0\sigma_{11}w_1 + \sigma_{21}E_{1z} + B_0\sigma_{21}u_1 + \frac{s\sigma_{21}}{\sigma_{01}B_0}\left(\frac{\partial p}{\partial x}\right), \tag{2.4}$$

$$J_{1z} = \sigma_{11}\left(\frac{E_{1z}}{B_0} + u_1\right) - \sigma_{21}\left(\frac{E_{1x}}{B_0} - w_1\right) - \frac{s}{B_0}\left(1 - \frac{\sigma_{11}}{\sigma_{01}}\right)\left(\frac{\partial p}{\partial x}\right). \tag{2.5}$$

Region-II

$$\rho_2\frac{\partial u_2}{\partial t} = \rho_2\nu_2\frac{\partial^2 u_2}{\partial y^2} - \rho_2 v_0\frac{\partial u_2}{\partial y} - \left\{1 - \left(1 - \frac{\sigma_{12}}{\sigma_{02}}\right)s\right\} + \\ + \left\{-\left(E_{2z} + u_2B_0\right)\sigma_{12} + \left(E_{2x} - w_2B_0\right)\sigma_{22}\right\}B_0, \tag{2.6}$$

$$\rho_2\frac{\partial w_2}{\partial t} = \rho_2\nu_2\frac{\partial^2 w_2}{\partial y^2} - \rho_2 v_0\frac{\partial w_2}{\partial y} + \left(s\ \frac{\sigma_{22}}{\sigma_{02}}\right)\frac{\partial p}{\partial x} + \\ + \left\{\left(E_{2x} - w_2B_0\right)\sigma_{12} + \left(E_{2z} + u_2B_0\right)\sigma_{22}\right\}B_0, \tag{2.7}$$

$$\rho_2 c_{p2}\frac{\partial T_2}{\partial t} = \frac{c_{p2}\mu_2}{P_r}\frac{\partial^2 T_2}{\partial y^2} + \rho_2 v_0\frac{\partial T_2}{\partial y} + \mu_2\left[\left(\frac{\partial u_2}{\partial y}\right)^2 + \left(\frac{\partial w_2}{\partial y}\right)^2\right] + \frac{J_2^2}{\sigma_{02}}, \tag{2.8}$$

$$J_{2x} = \sigma_{12}E_{2x} - B_0\sigma_{12}w_2 + \sigma_{22}E_{2z} + B_0\sigma_{22}u_2 + \frac{s\sigma_{22}}{\sigma_{02}B_0}\left(\frac{\partial p}{\partial x}\right), \tag{2.9}$$

$$J_{2z} = \sigma_{12}E_{2z} + \sigma_{12}B_0u_2 - \sigma_{22}E_{2x} + \sigma_{22}B_0w_2 - \frac{s}{B_0}\left(1 - \frac{\sigma_{12}}{\sigma_{02}}\right)\left(\frac{\partial p}{\partial x}\right). \tag{2.10}$$

In the aforementioned equations, 1 and 2 subscripts denote, respectively, the amounts for Regions-I and II. The values u_1, u_2 and w_1, w_2 represent, respectively, the primary and secondary velocity distributions for the two fluids and these are the *x*- and *z*-direction velocity components. Specifically, the *x*- and *z*-components of the electric field and current densities are denoted by the symbols E_{ix}, E_{iz}, and J_{ix}, J_{iz}. The ratio of the electron pressure to the total pressure is denoted by $s = p_e / p$. For neutral, completely ionized plasma, the estimation of s is *1/2*, while for a weakly ionized gas, it is close to zero. σ_{11}, σ_{12} and σ_{21}, σ_{22} are modified conductivities and are parallel to and normal to the direction of the electric field, respectively. Fluid velocity and sheer stress must be continuous over the interface at $y = 0$. The boundary and interface conditions on u_1, w_1 and u_2, w_2 and for the fluids in the two zones are given by the following equations:

$$\begin{aligned} u_1(h_1) \text{ and } w_1(h_1) &= 0 && \text{when } t \le 0, \\ &= \text{Real of } \varepsilon e^{i\omega t} && \text{when } t > 0. \end{aligned} \tag{2.11}$$

$$u_2(-h_2) = 0,\ w_2(-h_2) = 0, \tag{2.12}$$

$$u_1(0) = u_2(0), w_1(0) = w_2(0), \tag{2.13}$$

$$\mu_1 \frac{\partial u_1}{\partial y} = \mu_2 \frac{\partial u_2}{\partial y} \quad \text{and} \, \mu_1 \frac{\partial w_1}{\partial y} = \mu_2 \frac{\partial w_2}{\partial y} \ \text{at} \ h_1 = h_2. \tag{2.14}$$

For both fluids, the isothermal boundary and interface conditions for temperature are:

$$\begin{gathered} T_1(h_1) = T_{w1},\ T_2(-h_2) = T_{w2},\ T_1(0) = T_2(0), \\ K_1 \frac{\partial T_1}{\partial y} = K_2 \frac{\partial T_2}{\partial y} \quad \text{for} \quad h_1 = h_2 \ \text{(interface)}. \end{gathered} \tag{2.15}$$

To form Eqs (2.1) to (2.10) and (2.11) to (2.14) as dimensionless, the following non-dimensional variables are used:

$$\begin{gathered} u^{\bullet}_i = \frac{u_i}{u_p}, w^{\bullet}_i = \frac{w_i}{u_p}, y^{\bullet}_i = \frac{y_i}{h_i}, u_p = -\frac{\partial p}{\partial x}\frac{h_1^2}{\mu_1}, t^{\bullet} = \frac{\mu_i t}{\rho_i h_i^2}, \omega^{\bullet} = \frac{\omega h_i^2 \rho_i}{\mu_i}, \\ m_{ix} = \frac{E_{ix}}{B_0 u_p}, \quad m_{iz} = \frac{E_{iz}}{B_0 u_p}, I_{ix} = \frac{J_{ix}}{\sigma_{0i} B_0 u_p}, I_{iz} = \frac{J_{iz}}{\sigma_{0i} B_0 u_p}, \\ J_i^2 = J_{ix}^2 + J_{iz}^2, M = \sqrt{B^2{}_0 h^2{}_1 \left(\frac{\sigma_{01}}{\mu_1}\right)}, \lambda = \frac{h_1 \rho_1 v_0}{\mu_1}, \\ \alpha = \frac{\mu_1}{\mu_2}, h = \frac{h_2}{h_1}, \rho = \frac{\rho_2}{\rho_1}, \sigma_0 = \frac{\sigma_{01}}{\sigma_{02}}, \sigma_{01} = \frac{\sigma_{12}}{\sigma_{11}}, \sigma_{02} = \frac{\sigma_{22}}{\sigma_{21}}, \\ \frac{\sigma_{11}}{\sigma_{01}} = \frac{1}{1+m^2}, \frac{\sigma_{21}}{\sigma_{01}} = \frac{m}{1+m^2}, m = \frac{\omega_e}{\left(\frac{1}{\tau} + \frac{1}{\tau_e}\right)}, \beta = \frac{K_1}{K_2}, \theta_i = \frac{T_i - T_{wi}}{\left(u_p{}^2 \mu_1 / K_i\right)}. \end{gathered} \tag{2.16}$$

where $(i = 1,2)$, θ_i is the temperature distribution of the fluids, M is the Hartmann number, α is the viscosity ratio, h is the height ratio, ρ is the density, σ_0 is the electrical conductivity ratio, m is the Hall parameter and β is the thermal conductivity ratio between the two fluids. ω_e is the electron gyration frequency, τ and τ_e are the mean collision times between electron and neutron and electron and ion, respectively. Additionally, the previously stated formulation in (2.16) for the Hall parameter m, which is crucial due to partially-ionized gas, accords with the formulation for fully-ionized gas as τ_e approaches infinity.

The non-dimensional kinds of Eqs (2.1) through (2.14) are given by omitting the asterisks and considering transformations (2.16).

Region-I

$$\frac{\partial u_1}{\partial t}+\lambda\frac{\partial u_1}{\partial y}=\frac{\partial^2 u_1}{\partial y^2}-\left(\frac{M^2}{1+m^2}\right)\left(m_{1z}+u_1\right)+\left(\frac{mM^2}{1+m^2}\right)\left(m_{1x}-w_1\right)+k_1, \tag{2.17}$$

$$\frac{\partial w_1}{\partial t}+\lambda\frac{\partial w_1}{\partial y}=\frac{\partial^2 w_1}{\partial y^2}+\left(\frac{M^2}{1+m^2}\right)\left(m_{1x}-w_1\right)+\left(\frac{mM^2}{1+m^2}\right)\left(m_{1z}+u_1\right)+k_2, \tag{2.18}$$

$$\frac{\partial \theta_1}{\partial t}=\frac{1}{P_r}\frac{\partial^2\theta_1}{\partial y^2}+\lambda\frac{\partial\theta_1}{\partial y}+\left\{\left(\frac{\partial u_1}{\partial y}\right)^2+\left(\frac{\partial w_1}{\partial y}\right)^2+M^2{I_1}^2\right\}, \tag{2.19}$$

$$I_{1x}=\left(\frac{1}{1+m^2}\right)\left(m_{1x}-w_1\right)+\left(\frac{m}{1+m^2}\right)\left(m_{1z}+u_1\right)-\frac{s}{M^2}\left(\frac{m}{1+m^2}\right), \tag{2.20}$$

$$I_{1z}=\left(\frac{1}{1+m^2}\right)\left(m_{1z}+u_1\right)-\left(\frac{m}{1+m^2}\right)\left(m_{1x}-w_1\right)+\frac{s}{M^2}\left(1-\frac{m}{1+m^2}\right), \tag{2.21}$$

$${I_1}^2={I_{1x}}^2+{I_{1z}}^2.$$

Region-II

$$\frac{\partial u_2}{\partial t}+\rho\alpha h\lambda\frac{\partial u_2}{\partial y}=\frac{\partial^2 u_2}{\partial y^2}-\left(\frac{1}{1+m^2}\right)\alpha\sigma_1 h^2M^2\left(m_{2z}+u_2\right)+$$
$$+\left(\frac{m}{1+m^2}\right)\alpha\sigma_2 h^2M^2\left(m_{2x}-w_2\right)+\beta_1\alpha h^2, \tag{2.22}$$

$$\frac{\partial w_2}{\partial t}+\rho\alpha h\lambda\frac{\partial w_2}{\partial y}=\frac{\partial^2 w_2}{\partial y^2}+\left(\frac{1}{1+m^2}\right)\alpha\sigma_1 h^2M^2\left(m_{2x}-w_2\right)+$$
$$+\left(\frac{m}{1+m^2}\right)\alpha\sigma_2 h^2M^2\left(m_{2z}+u_2\right)+\beta_2\alpha h^2, \tag{2.23}$$

$$\frac{\partial \theta_2}{\partial t}=\frac{1}{P_r}\frac{\partial^2\theta_2}{\partial y^2}+\lambda\frac{\partial\theta_2}{\partial y}+\frac{\beta}{\alpha}\left[\left(\frac{\partial u_2}{\partial y}\right)^2+\left(\frac{\partial w_2}{\partial y}\right)^2\right]+\beta\sigma h^2M^2{I_2}^2, \tag{2.24}$$

$$I_{2x}=\left(\frac{\sigma_0\sigma_{01}}{1+m^2}\right)\left(m_{2x}-w_2\right)+\left(\frac{m\sigma_0\sigma_{02}}{1+m^2}\right)\left(m_{2z}+u_2\right)-\frac{s{\sigma_0}^2\sigma_{02}}{M^2}\left(\frac{m}{1+m^2}\right), \tag{2.25}$$

$$I_{2z}=\left(\frac{\sigma_0\sigma_{01}}{1+m^2}\right)\left(m_{2z}+u_2\right)-\left(\frac{m\sigma_0\sigma_{02}}{1+m^2}\right)\left(m_{2x}-w_2\right)+\frac{s\sigma_0}{M^2}\left(1-\frac{\sigma_0\sigma_{01}}{1+m^2}\right), \tag{2.26}$$

$$I_2^{\,2} = I_{2x}^{\,2} + I_{2z}^{\,2}$$

where, $k_1 = 1 - s\left(\frac{m^2}{1+m^2}\right)$, $k_2 = \frac{-sm}{1+m^2}$, $\beta_1 = 1 - s\left(1 - \frac{\sigma_0\sigma_{01}}{1+m^2}\right)$, $\beta_2 = \left(\frac{-s\sigma_0\sigma_{02}m}{1+m^2}\right)$.

The boundary and interface conditions on u_1, w_1 and u_2, w_2 are simplified as

$$u_1(1) = 0, \text{ for } t \le 0, \quad w_1(1) = 0, \quad \text{for } t \le 0,$$
$$u_1(1) = \varepsilon\cos\omega t, \text{ for } t > 0, \quad w_1(1) = \varepsilon\cos\omega t, \quad \text{for } t > 0, \tag{2.27}$$

$$u_2(-1) = 0, \; w_2(-1) = 0, \tag{2.28}$$

$$u_1(0) = u_2(0), \; w_1(0) = w_2(0), \tag{2.29}$$

$$\frac{\partial u_1}{\partial y} = \left(1/\alpha h\right)\frac{\partial u_2}{\partial y} \text{ and } \frac{\partial w_1}{\partial y} = \left(1/\alpha h\right)\frac{\partial w_2}{\partial y} \text{ and } \mu_1\frac{\partial w_1}{\partial y} = \mu_2\frac{\partial w_2}{\partial y} \text{ at } y = 0. \tag{2.30}$$

The isothermal boundary and the interface conditions are given by

$$\theta_1(1) = 0, \; \theta_2(-1) = 0, \; \theta_1(0) = \theta_2(0) \text{ and } \frac{\partial\theta_1}{\partial y} = \frac{1}{\beta h}\frac{\partial\theta_2}{\partial y} \quad \text{at } y = 0. \tag{2.31}$$

3. Method of solution

The momentum and energy equations (2.17)-(2.19) and (2.22)-(2.31) must be resolved in order to satisfy the boundary and interface conditions (2.27)-(2.31) for the velocity and temperature distributions in both fluid regions. Given that they are coupled partial differential equations, these equations cannot be solved in closed form. However, if the subsequent two-term series is assumed (Regular perturbation technique of first order), they can be reduced to simple linear differential equations [33].

$$u_1(y,t) = u_{01}(y) + \varepsilon\cos\omega t\, u_{11}(y) \quad \text{and } w_1(y,t) = w_{01}(y) + \varepsilon\cos\omega t\; w_{11}(y), \tag{3.1}$$

$$u_2(y,t) = u_{02}(y) + \varepsilon\cos\omega t\, u_{12}(y) \text{ and } w_2(y,t) = w_{02}(y) + \varepsilon\cos\omega t\; w_{12}(y), \tag{3.2}$$

$$\theta_1(y,t) = \theta_{01}(y) + \varepsilon\cos\omega t\; \theta_{11}(y) \text{ and } \theta_2(y,t) = \theta_{02}(y) + \varepsilon\cos\omega t\; \theta_{12}(y), \tag{3.3}$$

where the terms $u_{01}(y), u_{02}(y)$, $w_{01}(y), w_{02}(y)$ and $\theta_{01}(y)$, $\theta_{02}(y)$ are the temperature and velocity distributions in the steady-state two-fluid areas and $u_{11}(y)$, $u_{12}(y)$, $w_{11}(y)$, $w_{12}(y)$ and $\theta_{11}(y)$, $\theta_{12}(y)$ are the relevant time-dependent components.

We add the complex notation $q_1(y,t) = u_1(y,t) + iw_1(y,t)$ to unify Eqs (2.17) and (2.18) into a single equation and for convenience; likewise, $q_2(y,t) = u_2(y,t) + iw_2(y,t)$ to unify Eqs (2.22) and (2.23). We construct the differential equations by including the formulas from (3.1)-(3.3) into (2.17)-(2.19) and (2.22)-(2.24), then separate the steady and transient time-varying components. The boundary and interface conditions are used to resolve the resulting linear differential equations analytically. To find the conclusive

answers to the unstable EMHD problem in two-fluid regions, the closed form solutions for the steady and transient-time dependent sections are independently produced.
The solutions for the primary and secondary velocity distributions, u_1, u_2 and w_1, w_2, respectively, are provided by:

$$\begin{aligned} q_1(y,t) &= q_{01}(y) + \varepsilon \cos \omega t . q_{11}(y) \\ &= f_1 e^{f_{30} y} + f_2 e^{f_{31} y} + \frac{c_2}{c_1} + \varepsilon \cos \omega t \left(f_5 e^{f_{34} y} + f_6 e^{f_{35} y} \right) \end{aligned} \tag{3.4}$$

$$\begin{aligned} q_2(y,t) &= q_{02}(y) + \varepsilon \cos \omega t . q_{12}(y) \\ &= f_3 e^{f_{32} y} + f_4 e^{f_{33} y} + \frac{c_4}{c_3} + \varepsilon \cos \omega t \left(f_7 e^{f_{36} y} + f_8 e^{f_{37} y} \right) \end{aligned} \tag{3.5}$$

where $q_{01} = u_{01} + i w_{01}$, $q_{11} = u_{11} + i w_{11}$, $q_{02} = u_{02} + i w_{02}$, $q_{12} = u_{12} + i w_{12}$, $u_1(y,t) = \dfrac{q_1(y,t) + \overline{q_1(y,t)}}{2}$,

$w_1(y,t) = \dfrac{q_1(y,t) - \overline{q_1(y,t)}}{2i}$, and similarly for $u_2(y,t)$ and $w_2(y,t)$.

Mean velocity distributions are

$$\begin{aligned} q_{1m} &= u_{1m} + i w_{1m} = f_1 c_{97} + f_2 c_{98} + \frac{c_2}{c_1} + f_{28}, \\ q_{2m} &= u_{2m} + i w_{2m} = f_3 c_{99} + f_4 c_{100} + \frac{c_4}{c_3} + f_{29} \end{aligned} \tag{3.6}$$

where $u_{1m} = \dfrac{q_{1m} + \overline{q_{1m}}}{2}$, $w_{1m} = \dfrac{q_{1m} - \overline{q_{1m}}}{2i}$, $u_{2m} = \dfrac{q_{2m} + \overline{q_{2m}}}{2}$, $w_{2m} = \dfrac{q_{2m} - \overline{q_{2m}}}{2i}$.

Therefore, using the aforementioned expressions (3.4)-(3.6), we independently solve the appropriate energy equations for the steady and transient time-dependent components. The following are the concluding answers for the temperature distribution between the two regions and the rate of heat transfer coefficients at the channel porous plates under an unsteady condition:

Region-I:

$$\begin{aligned} \theta_1(y,t) &= \theta_{01}(y) + \varepsilon \cos \omega t \, \theta_{11}(y) = g_1 + g_2 e^{-\lambda y} - \left(d_{36} e^{d_{23} y} + d_{37} e^{d_{24} y} + \right. \\ &+ d_{38} e^{d_{25} y} + d_{39} e^{d_{26} y} + d_{40} e^{f_{30} y} + d_{41} e^{f_{31} y} + d_{42} e^{\overline{f_{30}} y} + d_{43} e^{\overline{f_{31}} y} + d_{44} y \Big) \\ &+ \varepsilon \cos \omega t \left(g_5 e^{g_9 y} + g_6 e^{g_{10} y} + d_{146} e^{d_{138} y} + d_{147} e^{d_{139} y} + d_{148} e^{d_{140} y} + \right. \\ &+ d_{149} e^{d_{141} y} + d_{150} e^{f_{34} y} + d_{151} e^{f_{35} y} + d_{152} e^{\overline{f_{34}} y} + d_{153} e^{\overline{f_{35}} y} \Big). \end{aligned} \tag{3.7}$$

The upper plate coefficient of heat transfer rate $Nu_1 = -\dfrac{\partial \theta_1}{\partial y}$ at $y = 1$ is:

$$Nu_1 = -\begin{bmatrix} -\lambda g_2 e^{-\lambda} - \left(d_{36} d_{23} e^{d_{23}} + d_{37} d_{24} e^{d_{24}} + d_{38} d_{25} e^{d_{25}} + d_{39} d_{26} e^{d_{26}} + \right. \\ + d_{40} f_{30} e^{f_{30}} + d_{41} f_{31} e^{f_{31}} + d_{42} \overline{f_{30}} e^{\overline{f_{30}}} + d_{43} \overline{f_{31}} e^{\overline{f_{31}}} + d_{44} \left. \right) + \\ + \varepsilon \cos \omega t \left(g_5 g_9 e^{g_9} + g_6 g_{10} e^{g_{10}} + d_{146} d_{138} e^{d_{138}} + d_{147} d_{139} e^{d_{139}} + \right. \\ + d_{148} d_{140} e^{d_{140}} + d_{149} d_{141} e^{d_{141}} + d_{150} f_{34} e^{f_{34}} + d_{151} f_{35} e^{f_{35}} + \\ \left. d_{152} \overline{f_{34}} e^{\overline{f_{34}}} + d_{153} \overline{f_{35}} e^{\overline{f_{35}}} \right) \end{bmatrix}. \tag{3.8}$$

Region-II:

$$\begin{aligned} &\theta_2(y,t) = \theta_{02}(y) + \varepsilon \cos \omega t \; \theta_{12}(y) = g_3 + g_4 e^{-d_{45} y} - \left(d_{86} e^{d_{74} y} + d_{87} e^{d_{75} y} + \right. \\ &+ d_{88} e^{d_{76} y} + d_{89} e^{d_{77} y} + d_{90} e^{f_{32} y} + + d_{91} e^{f_{33} y} + d_{92} e^{\overline{f_{32}} y} + d_{93} e^{\overline{f_{33}} y} + d_{94} y + \\ &+ \varepsilon \cos \omega t \left(g_7 e^{g_{11} y} + g_8 e^{g_{12} y} + d_{193} e^{d_{185} y} + d_{194} e^{d_{186} y} + d_{195} e^{d_{187} y} + \right. \\ &\left. + d_{196} e^{d_{188} y} + d_{197} e^{f_{36} y} + d_{198} e^{f_{37} y} + d_{199} e^{\overline{f_{36}} y} + d_{200} e^{\overline{f_{37}} y} \right). \end{aligned} \tag{3.9}$$

The lower plate coefficient of the heat transfer rate $Nu_2 = \dfrac{1}{\beta h} \dfrac{d\theta_2}{dy}$ at $y = -1$ is given by:

$$Nu_2 = \frac{1}{\beta h} \begin{bmatrix} -g_4 d_{45} e^{d_{45}} - \left(d_{86} d_{74} e^{-d_{74}} + d_{87} d_{75} e^{-d_{75}} + d_{88} d_{76} e^{-d_{76}} + d_{89} d_{77} e^{-d_{77}} + \right. \\ + d_{90} f_{32} e^{-f_{32}} + d_{91} f_{33} e^{-f_{33}} + d_{92} \overline{f_{32}} e^{-\overline{f_{32}}} + d_{93} \overline{f_{33}} e^{-\overline{f_{33}}} - d_{94} \left. \right) + \\ + \varepsilon \cos \omega t \left(g_7 g_{11} e^{-g_{11}} + g_8 g_{12} e^{-g_{12}} + d_{193} d_{185} e^{-d_{185}} + \right. \\ d_{194} d_{186} e^{-d_{186}} + d_{195} d_{187} e^{-d_{187}} + d_{196} d_{188} e^{-d_{188}} + d_{197} f_{36} e^{-f_{36}} + \\ \left. d_{198} f_{37} e^{-f_{37}} + d_{199} \overline{f_{36}} e^{-\overline{f_{36}}} + d_{200} \overline{f_{37}} e^{-\overline{f_{37}}} \right) \end{bmatrix} \tag{3.10}$$

where, the symbols and notations which are used to perform the mathematical analysis and make equations simpler are shown separately in the Appendix.

4.Results and Discussion:

The governing partial differential equations for the primary and secondary velocity distributions (u_1, u_2 and w_1, w_2) as well as the temperature distributions (θ_1, θ_2) in the two regions are solved using a two-term series (regular perturbation technique of first order). Graphical examples are used to explain related computational estimation for the various sets of governing parameter values. Figures 2 to 25 display profiles for the temperature and velocity distributions in the two zones as well as the rate of heat transfer coefficients. The profiles for unsteady motions are shown in the figures as solid lines, whereas those for steady motions

are dashed-spot lines. The impact of flow parameters on the velocity and temperature fields is explored by the Hartmann number *M*, Hall parameter *m*, porous parameter λ, density ratio ρ, viscosity ratio α, height ratio *h*, electrical conductivity ratio σ_0 and thermal conductivity ratio β. Since the issue involves a too many non-dimensional parameters, we fix the parameters $\sigma_{01} = 1.2$ and $\sigma_{02} = 1.5$ in all numerical computations for simplicity, and the effect of other significant parameters is examined. It is noticed that the solutions are found to be free of '*s*' (electron pressure to aggregate pressure proportion). We see that, when the motion is steady state and the channel side plates are non-porous, the analysis is in excellent agreement with the results of L.Raju [29]. Additionally, this analysis supports L.Raju and Gowri [33] solutions to the unsteady issue with non-porous side plates.

Figures 2, 3 and 4 illustrate how changing the Hartmann number *M* affects velocity and temperature distributions while all other parameters are held constant. As is seen in Fig.2, the primary velocity distribution diminishes when the Hartmann *M* augments up to an estimate of $M = 6$, beyond which it enhances in zone I. The primary velocity distribution in area II increases as the Hartmann number *M* rises until an estimate of $M = 4$, at which time it starts to fall. The secondary velocity distribution is shown in Fig.3 to grow with *M* up to an estimated value of $M = 6$, after which it decreases in the two zones. This tendency may be due to the Lorentz force actually which acts against the flow in the presence of a transverse magnetic field in an electrically conducting fluids. As *M* rises, the channel's most extreme primary and secondary velocity distributions have a tendency to move away from region-I (which is in the upper fluid area) over the channel's central line. It is found from Fig.4 that the temperature distribution in two regions decrease as *M* rises. The channel's most extreme temperature tends to shift beyond the channel focus line and toward region-I with an increase in the magnetic parameter *M*. These observations indicate that the applied transverse magnetic field has a more noticeable effect on velocity fields rather than temperature.

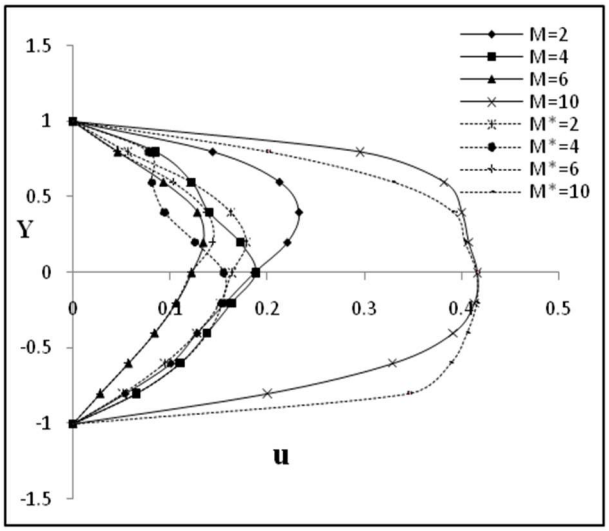

Fig.2. Velocity profiles (primary): unsteady flow u_1, u_2 and steady case u_1^*, u_2^* for varied M with $m = 2,\ \lambda = 2,\ \alpha = 0.333,\ h = 1,\ \sigma_0 = 2,\ \sigma_{01} = 1.2,\ \sigma_{02} = 1.5,\ \varepsilon = 0.5,\ \rho = 1,\ \omega = 1,\ t = \pi / \omega$. (Insulating porous plates).

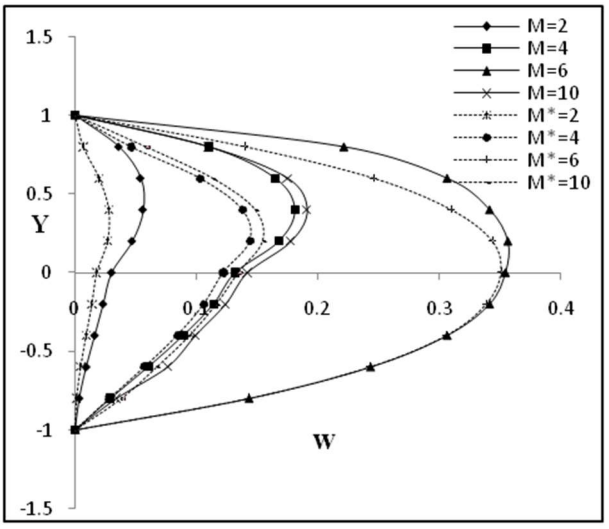

Fig.3. Velocity profiles (secondary): unsteady flow w_1, w_2 and steady case w_1^*, w_2^* for varied M with $m = 2,\ \lambda = 2,\ \alpha = 0.333,\ h = 1,\ \sigma_0 = 2,\ \sigma_{01} = 1.2,\ \sigma_{02} = 1.5,\ \varepsilon = 0.5,\ \rho = 1,\ \omega = 1,\ t = \pi / \omega$. (Insulating porous plates).

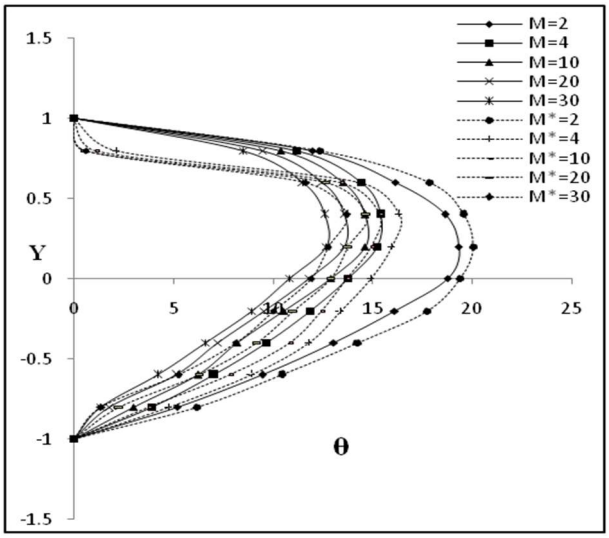

Fig.4. Temperature profiles: unsteady flow θ_1, θ_2 and steady case θ_1*, θ_2 * for varied M with $m = 2$, $\lambda = 2$, $\alpha = 0.333$, $h = 0.75$, $\sigma_0 = 2$, $\sigma_{01} = 1.2$, $\sigma_{02} = 1.5$, $\beta = 1$, $\varepsilon = 0.5$, $\rho = 1$, $\omega = 1$, $t = \pi / \omega$. (Insulating porous plates).

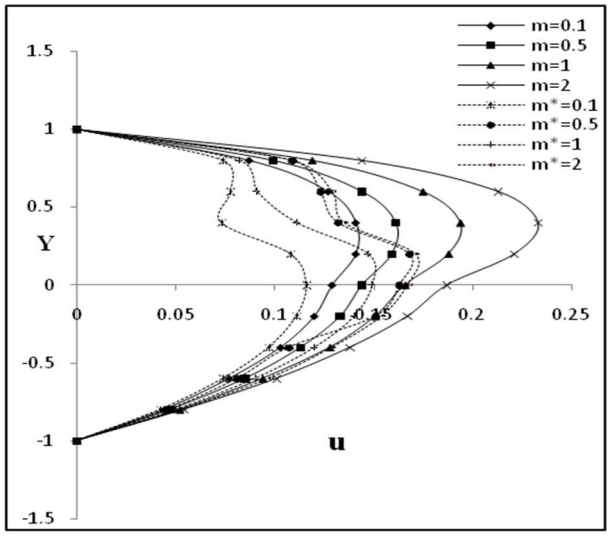

Fig.5. Velocity profiles (primary): unsteady flow u_1, u_2 and steady case u_1*, u_2 * for varied m with $M = 2$, $\lambda = 2$, $\alpha = 0.333$, $h = 1$, $\sigma_0 = 2$, $\sigma_{01} = 1.2$, $\sigma_{02} = 1.5$, $\varepsilon = 0.5$, $\rho = 1$, $\omega = 1$, $t = \pi / \omega$. (Insulating porous plates).

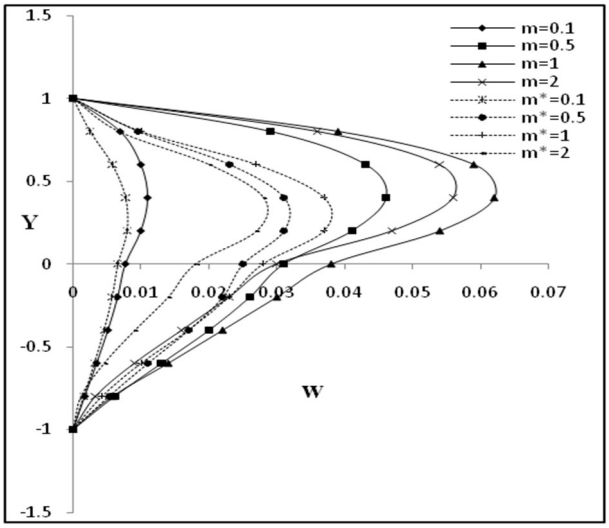

Fig.6. Velocity profiles (secondary): unsteady flow u_1, u_2 and steady case u_1*, u_2 * for varied m with $M = 2$, $\lambda = 2$, $\alpha = 0.333$, $h = 1$, $\sigma_0 = 2$, $\sigma_{01} = 1.2$, $\sigma_{02} = 1.5$, $\varepsilon = 0.5$, $\rho = 1$, $\omega = 1$, $t = \pi / \omega$. (Insulating porous plates).

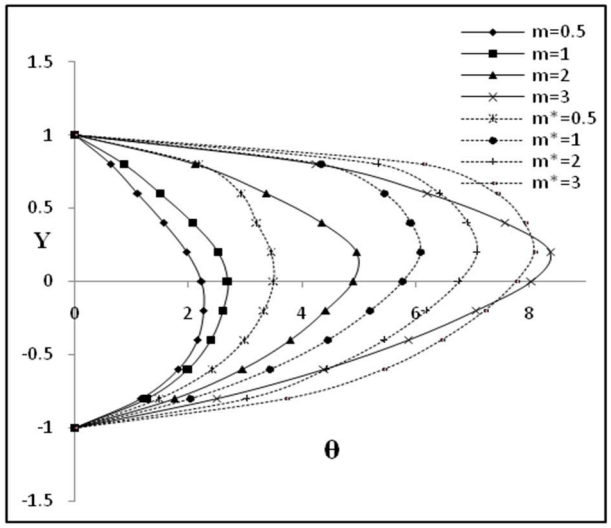

Fig.7. Temperature profiles: unsteady flow θ_1, θ_2 and steady case θ_1*, θ_2 * for varied m with $M = 4$, $\lambda = 2$, $\alpha = 0.333$, $h = 0.75$, $\sigma_0 = 2$, $\sigma_{01} = 1.2$, $\sigma_{02} = 1.5$, $\beta = 1$, $\varepsilon = 0.5$, $\rho = 1$, $\omega = 1$, $t = \pi / \omega$. (Insulating porous plates).

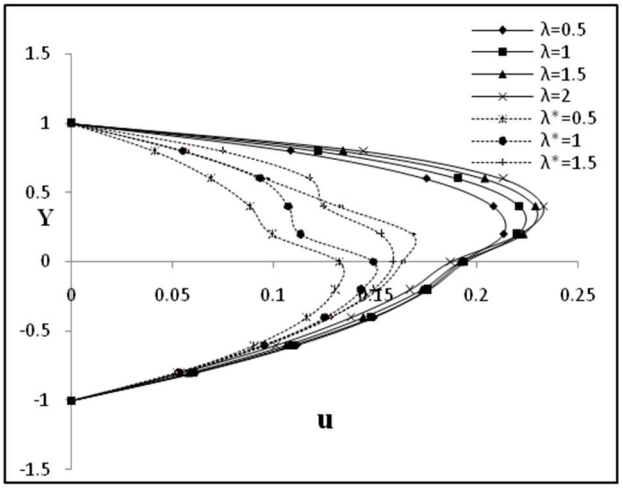

Fig.8. Velocity profiles (primary): unsteady flow u_1, u_2 and steady case u_1^*, u_2^* for varied λ with $M = 2,\ m = 2,\ \alpha = 0.333,\ h = 1,\ \sigma_0 = 2,\ \sigma_{01} = 1.2,$ $\sigma_{02} = 1.5,\ \varepsilon = 0.5,\ \rho = 1,\ \omega = 1,\ t = \pi / \omega.$ (Insulating porous plates).

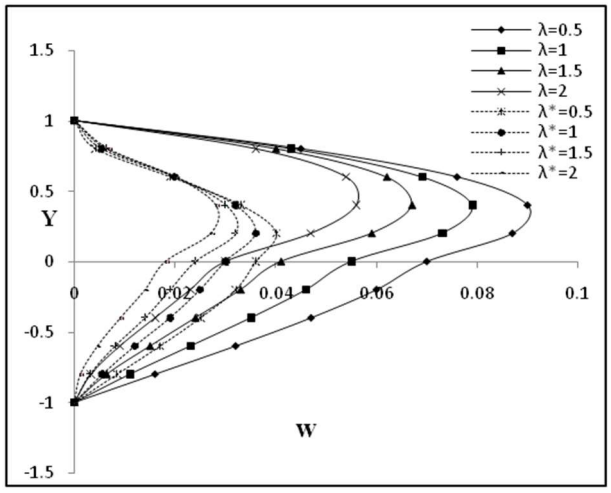

Fig.9. Velocity profiles (secondary): unsteady flow u_1, u_2 and steady case u_1^*, u_2^* for varied λ with $M = 2,\ m = 2,\ \alpha = 0.333,\ h = 1,\ \sigma_0 = 2,\ \sigma_{01} = 1.2,$ $\sigma_{02} = 1.5,\ \varepsilon = 0.5,\ \rho = 1,\ \omega = 1,\ t = \pi / \omega.$ (Insulating porous plates).

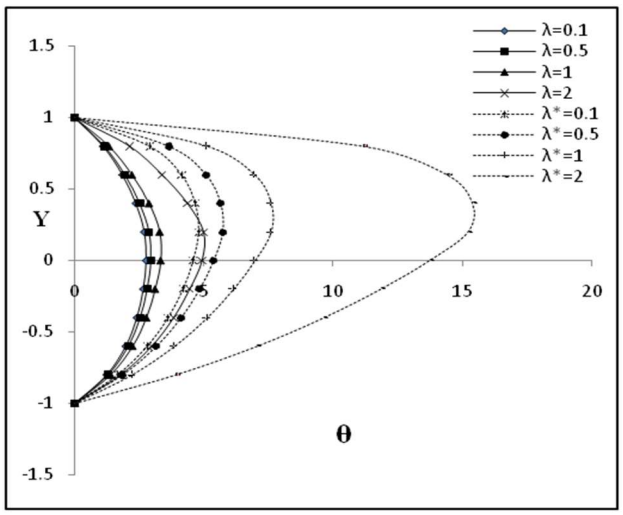

Fig.10. Temperature profiles: unsteady flow θ_1, θ_2 and steady case θ_1^*, θ_2^* for varied λ with $M = 4,$ $m = 2,\ \alpha = 0.333,\ h = 0.75,\ \sigma_0 = 2,\ \sigma_{01} = 1.2,$ $\sigma_{02} = 1.5,\ \beta = 1,\ \varepsilon = 0.5,\ \rho = 1,\ \omega = 1,\ t = \pi / \omega.$ (Insulating porous plates).

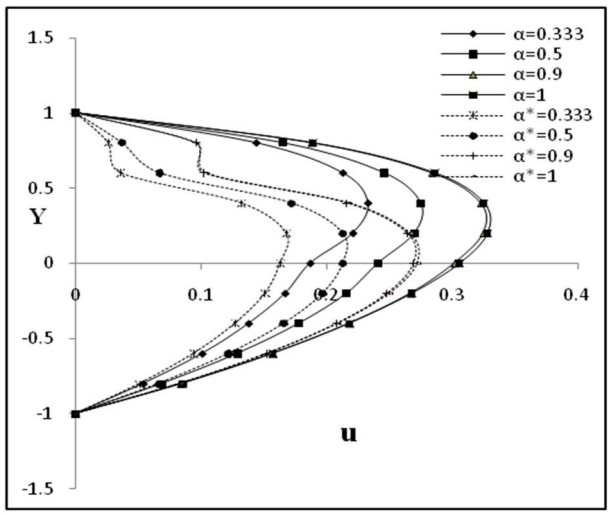

Fig.11. Velocity profiles (primary): unsteady flow u_1, u_2 and steady case u_1^*, u_2^* for varied α with $M = 2,\ m = 2,\ \lambda = 2,\ h = 1,\ \sigma_0 = 2,\ \sigma_{01} = 1.2,$ $\sigma_{02} = 1.5,\ \varepsilon = 0.5,\ \rho = 1,\ \omega = 1,\ t = \pi / \omega.$ (Insulating porous plates)

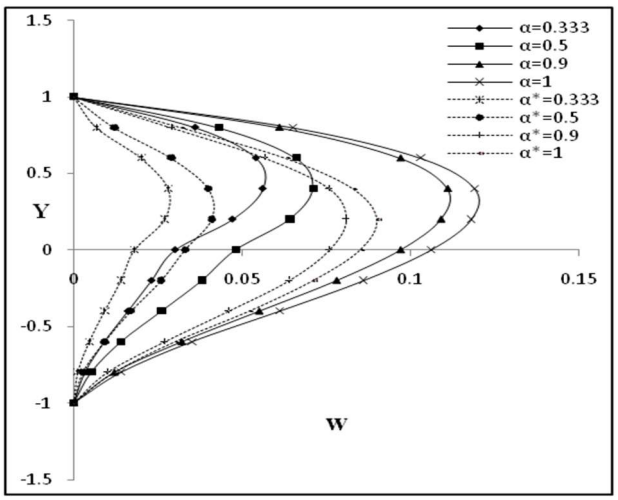

Fig.12 Velocity profiles (secondary): unsteady flow u_1, u_2 and steady case u_1^*, u_2^* for varied α with $M = 2,\ m = 2,\ \lambda = 2,\ h = 1,\ \sigma_0 = 2,\ \sigma_{01} = 1.2,\ \sigma_{02} = 1.5,\ \varepsilon = 0.5,\ \rho = 1,\ \omega = 1,\ t = \pi / \omega$. (Insulating porous plates).

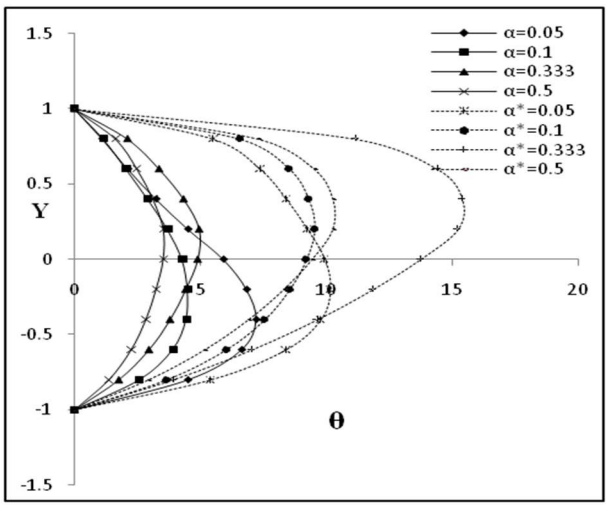

Fig.13 Temperature profiles: unsteady flow θ_1, θ_2 and steady case θ_1^*, θ_2^* for varied α with $M = 4,\ m = 2,\ \lambda = 2,\ h = 0.75,\ \sigma_0 = 2,\ \sigma_{01} = 1.2,\ \sigma_{02} = 1.5,\ \beta = 1,\ \varepsilon = 0.5,\ \rho = 1,\ \omega = 1,\ t = \pi / \omega$. (Insulating porous plates)

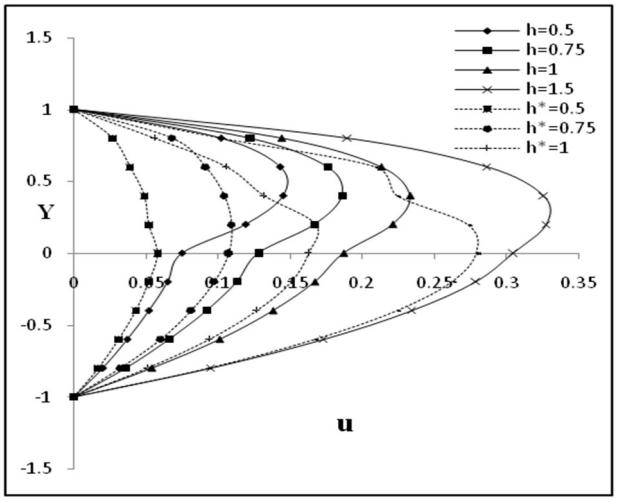

Fig.14. Velocity profiles (primary): unsteady flow u_1, u_2 and steady case u_1^*, u_2^* for varied h with $M = 2,\ m = 2,\ \lambda = 2,\ \alpha = 0.333,\ \sigma_0 = 2,\ \sigma_{01} = 1.2,\ \sigma_{02} = 1.5,\ \varepsilon = 0.5,\ \rho = 1,\ \omega = 1,\ t = \pi / \omega$. (Insulating porous plates).

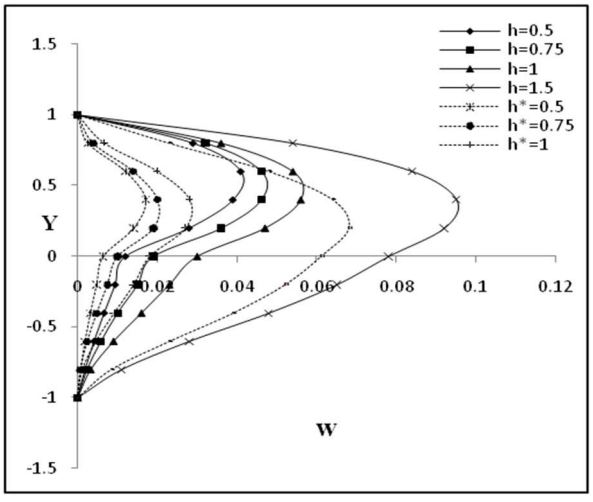

Fig.15. Velocity profiles (secondary): unsteady flow w_1, w_2 and steady case w_1^*, w_2^* for varied h with $M = 2,\ m = 2,\ \lambda = 2,\ \alpha = 0.333,\ \sigma_0 = 2,\ \sigma_{01} = 1.2,\ \sigma_{02} = 1.5,\ \varepsilon = 0.5,\ \rho = 1,\ \omega = 1,\ t = \pi / \omega$. (Insulating porous plates).

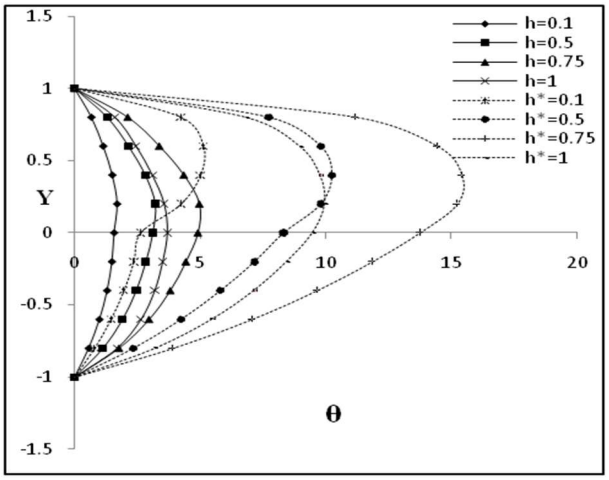

Fig.16. Temperature profiles: unsteady flow θ_1, θ_2 and steady case θ_1^*, θ_2^* for varied h with $M = 4$, $m = 2$, $\lambda = 2$, $\alpha = 0.333$, $\sigma_0 = 2$, $\sigma_{01} = 1.2$, $\sigma_{02} = 1.5$, $\beta = 1$, $\varepsilon = 0.5$, $\rho = 1$, $\omega = 1$, $t = \pi / \omega$. (Insulating porous plates).

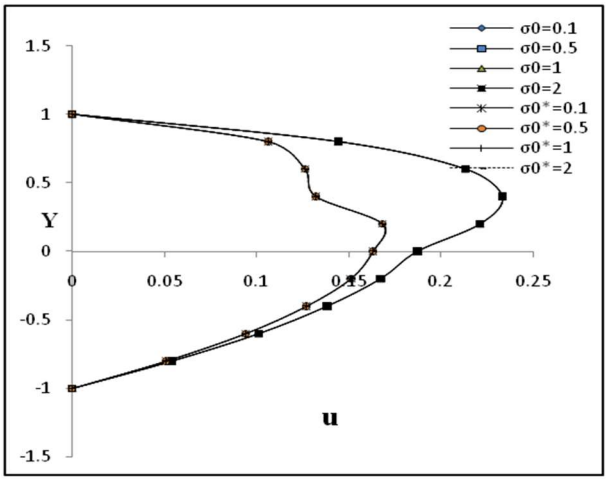

Fig.17. Velocity profiles (primary): unsteady flow u_1, u_2 and steady case u_1^*, u_2^* for varied σ_0 with $M = 2$, $m = 2$, $\lambda = 2$, $\alpha = 0.333$, $h = 1$, $\sigma_{01} = 1.2$, $\sigma_{02} = 1.5$, $\varepsilon = 0.5$, $\rho = 1$, $\omega = 1$, $t = \pi / \omega$. (Insulating porous plates).

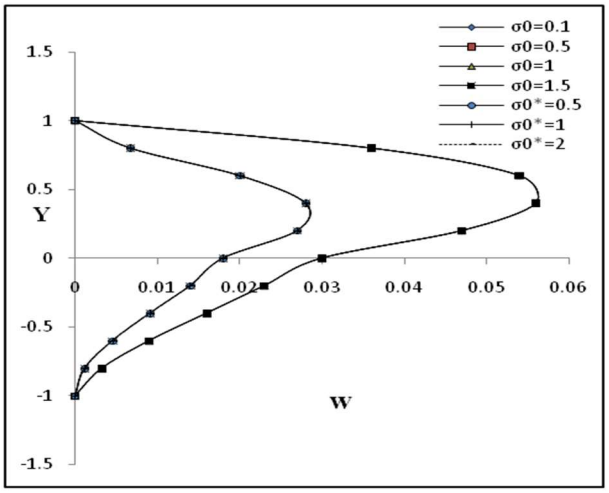

Fig.18 Velocity profiles (secondary): unsteady flow u_1, u_2 and steady case u_1^*, u_2^* for varied σ_0 with $M = 2$, $m = 2$, $\lambda = 2$, $\alpha = 0.333$, $h = 1$, $\sigma_{01} = 1.2$, $\sigma_{02} = 1.5$, $\varepsilon = 0.5$, $\rho = 1$, $\omega = 1$, $t = \pi / \omega$. (Insulating porous plates).

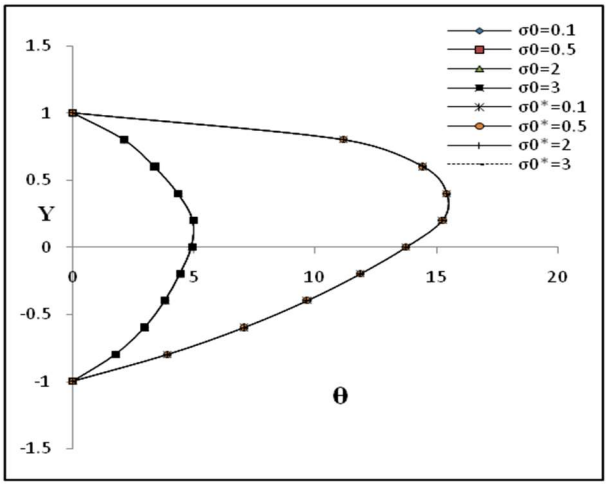

Fig.19. Temperature profiles: unsteady flow θ_1, θ_2 and steady case θ_1^*, θ_2^* for varied σ_0 with $M = 4$, $m = 2$, $\lambda = 2$, $\alpha = 0.333$, $h = 0.75$, $\sigma_{01} = 1.2$, $\sigma_{02} = 1.5$, $\beta = 1$, $\varepsilon = 0.5$, $\rho = 1$, $\omega = 1$, $t = \pi / \omega$. (Insulating porous plates).

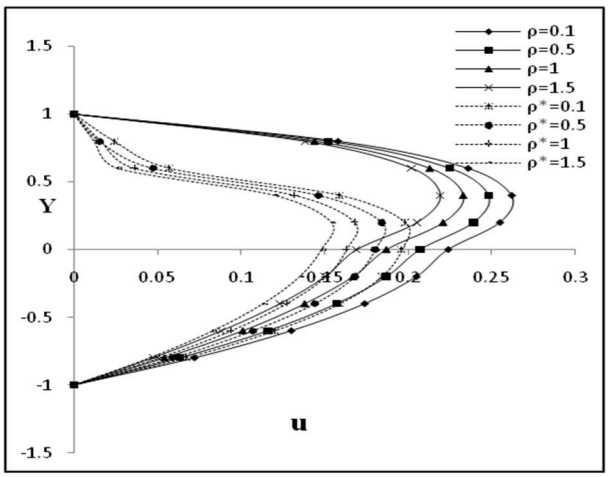

Fig.20. Velocity profiles (primary): unsteady flow u_1, u_2 and steady case u_1^*, u_2^* for varied ρ with $M = 2,\ m = 2,\ \lambda = 2,\ \alpha = 0.333,\ h = 1,\ \sigma_0 = 2,$ $\sigma_{01} = 1.2,\ \sigma_{02} = 1.5,\ \varepsilon = 0.5,\ \omega = 1,\ t = \pi / \omega.$ (Insulating porous plates).

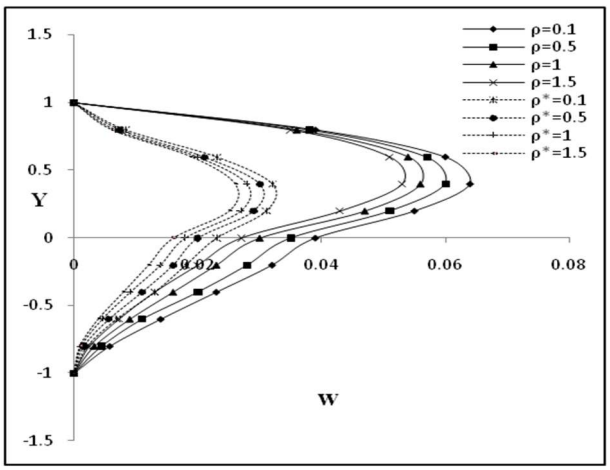

Fig.21. Velocity profiles (secondary): unsteady flow u_1, u_2 and steady case u_1^*, u_2^* for varied ρ with $M = 2,\ m = 2,\ \lambda = 2,\ \alpha = 0.333,\ h = 1,\ \sigma_0 = 2,$ $\sigma_{01} = 1.2,\ \sigma_{02} = 1.5,\ \varepsilon = 0.5,\ \rho = 1,\ \omega = 1,\ t = \pi / \omega.$ (Insulating porous plates).

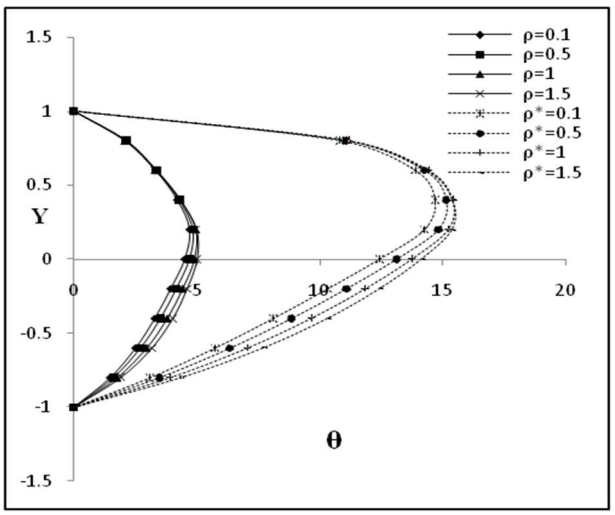

Fig.22 Temperature profiles: unsteady flow θ_1, θ_2 and steady case θ_1^*, θ_2^* for varied ρ with $M = 4,$ $m = 2,\ \lambda = 2,\ \alpha = 0.333,\ h = 0.75,\ \sigma_0 = 2,\ \sigma_{01} = 1.2,$ $\sigma_{02} = 1.5,\ \beta = 1,\ \varepsilon = 0.5,\ \rho = 1,\ \omega = 1,\ t = \pi / \omega.$ (Insulating porous plates).

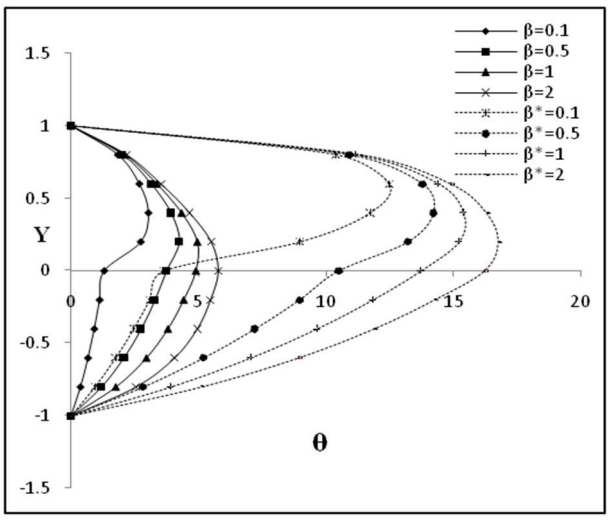

Fig.23 Temperature profiles: unsteady flow θ_1, θ_2 and steady case θ_1^*, θ_2^* for varied β with $M = 4,$ $m = 2,\ \lambda = 2,\ \alpha = 0.333,\ h = 0.75,\ \sigma_0 = 2,\ \sigma_{01} = 1.2,$ $\sigma_{02} = 1.5,\ \varepsilon = 0.5,\ \rho = 1,\ \omega = 1,\ t = \pi / \omega.$ (Insulating porous plates).

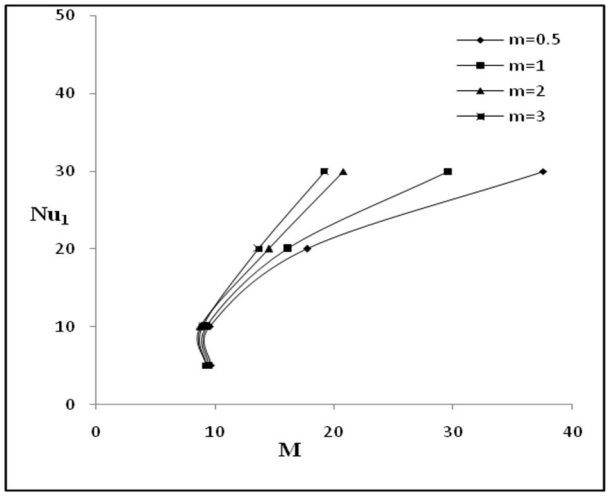

Fig.24. Nusselt Number (Nu_1) for varied M with $\lambda = 2,\ \alpha = 0.333,\ h = 0.75,\ \sigma_0 = 2,\ \sigma_{01} = 1.2,$ $\sigma_{02} = 1.5,\ \beta = 1,\ \varepsilon = 0.5,\ \rho = 1,\ \omega = 1,\ t = \pi / \omega.$ (Insulating porous plates).

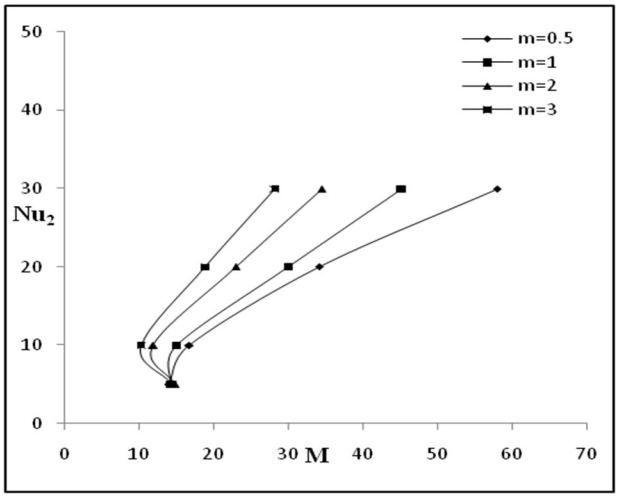

Fig.25. Nusselt Number (Nu_2) for varied M with $\lambda = 2,\ \alpha = 0.333,\ h = 0.75,\ \sigma_0 = 2,\ \sigma_{01} = 1.2,$ $\sigma_{02} = 1.5,\ \beta = 1,\ \varepsilon = 0.5,\ \rho = 1,\ \omega = 1,\ t = \pi / \omega.$ (Insulating porous plates).

Figures 5 and 6 show how changing the Hall parameter 'm' affects both primary and secondary velocity distributions. Figure 5 illustrates how increasing m improves the primary velocity distribution in the two locations. Figure 6 demonstrates that the secondary velocity distribution rises as m rises up to an estimated value of 1 before falling in the two locations. The highest primary and secondary velocity distributions of the channel are also seen to be moving over the channel center line and toward zone-I when m increments. The cause of the variable Hall parameter m on temperature field is seen in Fig.7. It is seen that raising m enhances how evenly the temperatures are distributed between the two regions. This implies that the Hall parameter accelerates the temperature of the fluids in the two locations. The channel's highest temperature also has a tendency to cross the channel center-line and move toward zone-I when m increases.

Figures 8, 9, and 10 each depict how the porosity parameter λ affects the distributions of velocity and temperature. Figure 8 illustrates how a drop in the primary velocity distribution in area II results from an increase in λ, whereas increasing λ leads the primary velocity distribution in Region-I to grow. A rising λ lowers the secondary velocity distribution in the two zones, as shown in Fig.9. Further investigation demonstrates that the greatest primary and secondary velocity distributions in the channel have a tendency to migrate toward region-I as λ increases by crossing the channel focus center line. From Fig.10, it is evident that the temperature circulation has increased in two zones. As a result, suction tends to higher temperature in both locations. As the permeability parameter λ raises, the channel's greatest temperature conveyance tends to migrate away from region-I and over the channel focal line.

Figures 11 and 12 show the results of the viscosities ratio α between the two liquids. In both zones, the primary and secondary velocity distributions are found to increase as α increases. As α increases, the channel's most extreme primary and secondary velocity distributions have a tendency to cross the channel focus line and head towards Region-I. Figure 13 shows the impact of the viscosity ratio α on the temperature distribution. The temperature distribution is observed to decrease as α increases up to $\alpha = 1$, after which it increases up to $\alpha = 0.3$ before decreasing once more close to the channel's centre. The temperature transmission decreases in Region-II. Additionally, when the viscosity proportion grows, the temperature distribution in the channel tends to shift towards Region-II, beneath the channel focus line.

Figures 14, 15 and 16 illustrate the effect of changing the height ratio h on velocity and temperature distributions. The primary and secondary velocity distributions in the two zones are seen to increase as h increases. The channel's most primary and secondary velocity distributions typically move with 'h'

increments over the channel centre line in the direction of Region-I. Figure 16 shows that increasing *h* increases the temperature dispersion up to h=0.75, after which the temperature dispersion in the two zones decreases. As *h* increases, the channel's highest temperature has a tendency to shift beyond the channel focus line and toward Region-I.

Figures 17, 18 and 19 display the impact of electrical conductivity ratio σ_0 on velocity and temperature fields. It is found that, when σ_0 increases; neither the primary nor secondary velocity distributions show any major or minor deviation. As σ_0 increases, the channel's maximum primary and secondary velocity distributions have a tendency to cross the channel focus line and head toward Region-I. It is found from Fig.19 that as σ_0 increases in the two zones, there is no significant minor deviation from temperature conveyance. As σ_0 increases, the channel's most extreme temperature dispersion has a tendency to cross the channel focus line and head toward zone-I.

Figures 20, 21 and 22 show how the density ratio ρ affects the distributions of velocity and temperature in the two fluid zones. It is seen from Figs 20 and 21 that an increase in ρ reduces the two regions' primary and secondary velocity distributions. As ρ increases, the channel's most extreme main and secondary velocity distributions have a tendency to cross the channel centre line and head in the direction of area I. It is found from Fig.22 that the temperature distribution in the two zones will be built by an increasing ρ. As ρ increases, the channel's highest temperature has a tendency to cross the channel focal line and head toward area I.

Figure23 shows the effect of thermal conductivity ratio β on temperature distribution. The temperature distribution in the two zones is observed to be increased by an increasing β. As β increases, the channel's highest temperature has a tendency to shift slightly over the focus line and toward region-I.

The rate of heat transmission coefficients in relation to the Hartmann number *M* is shown in Figs 24 and 25. It is clear that the rate of heat transfer increases as *M* grows when all governing factors are held constant. The rate of heat transfer at the plates is, however, reduced up to a certain value when the Hall parameter m is increased, and thereafter it increases.

5. Conclusions

Theoretically, Hall currents are used to study the behaviour of the temperature distribution brought on by an EMHD two liquid flow of ionized gases into a straight channel constructed of porous non-conducting plates. Graphs are used to investigate the effects of flow parameters on the temperature fields and rate of heat transfer coefficients in two liquid zones. These parameters include the Hartman number, Hall parameter, Porous parameter, ratios of the viscosities, densities, heights, electrical conductivities, and thermal conductivities. Some significant outcomes include the following:

- In zone-I, the primary velocity distribution increases up to an estimated value and then reduces past this estimate as the Hartmann number rises, where in zone-II, it enhances up to an estimated value and then decreases past this estimate. Up to a particular parameter estimation, the secondary velocity distribution increases, and then it starts to decline.
- As the Hartmann number rises, the temperature distribution in two regions becomes less uniform.
- The secondary distribution grows with an increase in the Hall parameter up to a certain estimate, after which it drops in the two regions. This contrasts with the main distribution, which is improved in both regions by an increasing Hall parameter.
- The temperature distribution in two regions is enhanced by an increase in the Hall parameter.
- An increment in the porous parameter enhances the primary velocity distribution in Region-I and diminishes in the Region-II, while the secondary velocity distribution diminishes in the two regions.
- A growth in either the Hall parameter/or porous parameter/or thermal conductivity ratio/or density ratio improves the dispersion of temperature in the two regions.

- A rise in the viscosity or density ratio or height ratio improves primary and secondary velocity profiles.
- When either the height ratio or viscosity ratio increases up to a certain point, the temperature distribution increases; after that, it decreases in the two zones.
- An increase in the Hartmann number accelerates the rate of heat transfer coefficients at the plates. However, as the Hall parameter increases up to a certain point, the rate of heat transfer coefficient at the plates decreases and from that point on, it increases.

Acknowledgments:

This research was supported by St. Joseph's College for Women(A), Visakhapatnam, (under Seed money project - a minor project), I thank our principal Dr. Sr. ShyjiP. D. and IQAC team. To my study supervisor, Prof. T. Linga Raju of Andhra University, I would like to convey words of my sincere gratitude for his patient supervision, enthusiastic support, and helpful criticism of my research endeavor. Without my supervisor's assistance, this paper and the research that went into it would not have been feasible.

Nomenclature

B_0 – applied magnetic field

$\overline{B}$ – magnetic flux intensity

$c_1, c_2, ..., d_1, d_2, ...$
$f_1, f_2, ..., g_1, g_2, ...$
$m_1,\ m_2,\ m_3 ...$ – symbols/or functional relations considered in all the solutions and equations.

$c_{pi}\,(i = 1,2)$ – specific heat in the two fluid regions at constant pressure

$E_{ix},\ E_{iz}, i = 1,2$ – applied electric fields in *x*- and *z*- directions respectively

h – height ratio

h_1 – height of upper region (Region-I)

h_2 – height of the lower region

I_{ix}, I_{iz} – current. densities in two fluid regions along the *x*- and *z*-axes those are dimensionless

$J_{ix},\ J_{iz}$ – current densities in the *x*- and *z*-axes, respectively

$\overline{J}$ – current density

K_1, K_2 – fluid's thermal conductivities

m – Hall parameter

$m_{ix},\ m_{iz}$ – electric fields with no dimensions of both fluid regions

M – Hartmann number

N_1, N_2 – represented symbols for $N_1 = m_{1x} + im_{1z}$ and $N_2 = m_{2x} + im_{2z}$

$Nu_1,\ Nu_2$ – heat transfer coefficients at upper and lower plates

P – pressure

p_e – electron pressure

$q_{01}, q_{02}, q_{11}, q_{12}$ – velocities in steady and transient states expressed in complex notation

$q_{1m},\ q_{2m}$ – mean velocities in complex notation, where $q_{1m} = u_{1m} + iw_{1m}, q_{2m} = u_{2m} + iw_{2m}$

$s = p_e / p$ –ionization number = ratio of electron pressure to total pressure

$t,\ T$ – time, temperature

$T_i\left(i=1,2\right):T_1,T_2$ – fluid's temperature for two regions

$u_i\left(i=1,2\right):u_1,u_2$ – primary velocity distributions

u_{1m},u_{2m} – mean primary velocity distributions

$u_{01}\left(y\right),u_{02}\left(y\right)$ – primary velocity distributions in steady state case

$u_{11}\left(y\right),u_{12}\left(y\right)$ – transient primary velocity components

u_p –characteristic velocity = $-\frac{\partial p}{\partial x}\frac{h_i^2}{\mu_i}$

$\overline{V_i}$ – fluid velocity

$w_i\left(i=1,2\right):w_1,w_2$ – secondary velocity distributions

w_{1m},w_{2m} – mean secondary velocities

$w_{01}\left(y\right),w_{02}\left(y\right)$ – steady state- secondary velocity distributions

$w_{11}\left(y\right),w_{12}\left(y\right)$ – transient state- secondary velocity components

$(x,y,z):$ – The rectangular Cartesian space coordinates

$\frac{\partial p}{\partial x}$ – common-constant pressure-gradient

α – viscosities proportion

β – thermal conductivities proportion

λ – porous parameter

$\mu_1,\ \mu_2$ – fluids' viscosities

σ_{01},σ_{02} – both fluids' electrical conductivities

σ_0 – electrical conductivity ratio

$\sigma_{11},\sigma_{12},\sigma_{21},\sigma_{22}$ – modified conductivities parallel and normal to the electric field's direction

σ_1,σ_2 – symbols used for $\sigma_1=\sigma_{12}/\sigma_{11},\sigma_2=\sigma_{22}/\sigma_{21}$

ε – amplitude (a small constant quantity, $\varepsilon << 1$)

ρ – ratio of densities

ρ_1,ρ_2 – the two fluids' densities

$\theta_1,\ \theta_2$ – non-dimensional temperature distributions

$\theta_{01}\left(y\right),\ \theta_{02}\left(y\right)$ – temperature distributions at steady state

$\theta_{11}\left(y\right),\ \theta_{12}\left(y\right)$ – temperature distributions during a transient state

$\tau,\ \tau_e$ – between an electron and an ion or an electron and a neutral particle, the average collision period

ω – oscillation frequency

ω_e – electron gyratory frequency

subscripts:

1, 2 – quantities indicate for both upper and lower fluid regions

Appendix

$$N_1 = m_{1x} + im_{1z}, \quad N_2 = m_{2x} + im_{2z}, \quad \lambda_1 = \rho\alpha h\lambda, \quad k_1 = 1 - s\left(\frac{m^2}{1+m^2}\right),$$

$$k_2 = \frac{-sm}{1+m^2}, \qquad \beta_1 = 1 - s\left(1 - \frac{\sigma_0\sigma_{01}}{1+m^2}\right), \quad \beta_2 = \frac{-s\sigma_0\sigma_{02}m}{1+m^2},$$

$$c_1 = M^2\left(\frac{mi-1}{1+m^2}\right), \quad c_2 = -\left\{f_9 + M^2N_1\left(\frac{i+m}{1+m^2}\right)\right\},$$

$$c_3 = -\alpha h^2M^2(\sigma_1 - mi\sigma_2)\frac{1}{1+m^2}, \quad c_4 = -\left\{f_{10}\alpha h^2 + \alpha h^2M^2N_2(i\sigma_1 + m\sigma_2)\frac{1}{1+m^2}\right\},$$

$$c_{97} = \frac{e^{f_{30}} - 1}{f_{30}}, \quad c_{98} = \frac{e^{f_{31}} - 1}{f_{31}}, \quad c_{99} = \frac{e^{f_{32}} - 1}{f_{32}}, \quad c_{100} = \frac{e^{f_{33}} - 1}{f_{33}},$$

$$d_{23} = f_{30} + \overline{f_{30}}, \quad d_{24} = f_{30} + \overline{f_{31}}, \quad d_{25} = f_{31} + \overline{f_{30}}, \quad d_{26} = f_{31} + \overline{f_{31}},$$

$$d_{40} = \frac{d_{31}}{f_{30}^2 + \lambda f_{30}}, \quad d_{42} = \frac{d_{33}}{\left(\overline{f_{30}}\right)^2 + \lambda\overline{f_{30}}}, \quad d_{43} = \frac{d_{34}}{\left(\overline{f_{31}}\right)^2 + \lambda\overline{f_{31}}},$$

$$d_{74} = f_{32} + \overline{f_{32}}, \quad d_{75} = f_{32} + \overline{f_{33}}, \quad d_{76} = f_{33} + \overline{f_{32}}, \quad d_{77} = f_{33} + \overline{f_{33}},$$

$$d_{92} = \frac{d_{84}}{\left(\overline{f_{32}}\right)^2 + d_{45}\overline{f_{32}}}, \quad d_{93} = \frac{d_{85}}{\left(\overline{f_{33}}\right)^2 + d_{45}\overline{f_{33}}}, \quad d_{134} = d_{123}\overline{f_5}, \quad d_{135} = d_{123}\overline{f_6},$$

$$d_{136} = d_{124}f_5, \quad d_{137} = d_{124}f_6, \quad d_{138} = f_{34} + \overline{f_{34}},$$

$$d_{158} = f_{34}^2 + \lambda f_{34} + d_{120}, \quad d_{159} = f_{35}^2 + \lambda f_{35} + d_{120}, \quad d_{160} = \left(\overline{f_{34}}\right)^2 + \lambda\overline{f_{34}} + d_{120},$$

$$d_{161} = \left(\overline{f_{35}}\right)^2 + \lambda\overline{f_{35}} + d_{120}, \quad d_{162} = \lambda\overline{f_{35}} + d_{120},$$

$$d_{163} = d_{55}\varepsilon^2\cos^2\omega t, \quad d_{164} = d_{56}\varepsilon^2\cos^2\omega t, \quad d_{165} = -d_{56}d_{53}\varepsilon\cos\omega t,$$

$$d_{166} = -d_{56}d_{54}\varepsilon\cos\omega t, \quad d_{167} = d_{166}\varepsilon\cos\omega t, \quad d_{168} = \frac{d_{163}}{d_{113}}, \quad d_{169} = \frac{d_{164}}{d_{113}},$$

$$d_{181} = d_{170}\overline{f_7}, \quad d_{182} = d_{170}\overline{f_8}, \; d_{185} = f_{36} + \overline{f_{36}}, \; d_{186} = f_{36} + \overline{f_{37}},$$

$$d_{187} = f_{37} + \overline{f_{36}}, \; d_{188} = f_{37} + \overline{f_{37}}, \; d_{285} = d_{273} + d_{277}, \; d_{286} = d_{274} + d_{278},$$

$$d_{287} = d_{275} + d_{279}, \; d_{288} = d_{276} + d_{280}, \quad d_{289} = \frac{d_{285}}{d_{138}^2 + \lambda d_{138} + d_{120}},$$

$$d_{290}=\frac{d_{286}}{d_{139}{}^2+\lambda d_{139}+d_{120}},\quad d_{291}=\frac{d_{287}}{d_{140}{}^2+\lambda d_{140}+d_{120}},$$

$$d_{292}=\frac{d_{288}}{d_{141}{}^2+\lambda d_{141}+d_{120}},\quad d_{293}=\frac{d_{281}}{\left(\overline{f}_{34}\right)^2+\lambda\overline{f}_{34}+d_{120}},\quad d_{294}=\frac{d_{282}}{\left(\overline{f}_{35}\right)^2+\lambda\overline{f}_{35}+d_{120}},$$

$$d_{295}=\frac{d_{283}}{f_{34}{}^2+\lambda f_{34}+d_{120}},\quad d_{296}=\frac{d_{284}}{f_{35}{}^2+\lambda f_{35}+d_{120}},\quad d_{297}=d_{55}d_{270},$$

$$d_{299}=d_{297}f_{36}f_7\overline{f}_7\overline{f}_{36},\quad d_{302}=d_{297}f_{37}f_8\overline{f}_{37}\overline{f}_8,\quad d_{332}=g_9d_{327}-d_{330}-\frac{g_{11}}{\beta h}d_{328}+\frac{d_{331}}{\beta h},$$

$$d_{337}=q_{m_1},\quad d_{338}=\overline{q}_{m_1},\quad d_{339}=\frac{1}{q_{m_1}\overline{q}_{m_1}},\quad d_{340}=\frac{M^2}{1+m^2}d_{339},\quad d_{341}=d_{339}f_{41}f_{30}f_{41}\overline{f}_{30},$$

$$d_{344}=d_{339}f_{42}f_{31}\overline{f}_{42}\overline{f}_{31},\quad d_{370}=\frac{d_{361}}{d_{25}{}^2+\lambda d_{25}},\quad d_{385}=d_{380}f_{43}\overline{f}_{43},\quad d_{386}=d_{380}f_{43}\overline{f}_{44},$$

$$d_{388}=d_{380}f_{44}\overline{f}_{43},\quad d_{389}=d_{380}f_{44}\overline{f}_{44},\quad d_{390}=d_{380}f_{44}\frac{\overline{c_4}}{c_{184}},\quad d_{391}=d_{380}\overline{f}_{43}\frac{c_4}{c_{184}},$$

$$d_{392}=d_{380}\overline{f}_{44}\frac{c_4}{c_{184}},\quad d_{393}=-d_{380}d_{377}\overline{f}_{33},\quad d_{394}=-d_{380}d_{377}\overline{f}_{44},\quad d_{395}=-d_{378}d_{380}f_{43},$$

$$d_{396}=-d_{378}d_{380}f_{44},\quad d_{397}=d_{380}\frac{c_4}{c_{184}}\frac{\overline{c_4}}{c_{184}}-d_{378}d_{380}\frac{c_4}{c_{184}}-d_{380}d_{377}\frac{\overline{c_4}}{c_{184}}+d_{380}d_{377}d_{378},$$

$$d_{398}=d_{381}+d_{385},\quad d_{399}=d_{382}+d_{386},\quad d_{400}=d_{383}+d_{388},\quad d_{401}=d_{384}+d_{389},$$

$$d_{402}=d_{387}+d_{395},\ d_{431}=\left(1-\frac{1}{1+m^2}\right)\frac{s^2}{M^2}d_{339},\ d_{432}=\frac{d_{427}}{d_{113}},$$

$$d_{437}=d_{432}f_5f_{34}\overline{f}_5\overline{f}_{34},\ d_{438}=d_{432}f_5\overline{f}_{34}\overline{f}_6\overline{f}_{35},\ d_{439}=d_{432}f_6f_{35}\overline{f}_5\overline{f}_{34},$$

$$d_{440}=d_{432}f_6f_{35}\overline{f}_6\overline{f}_{35},\ d_{441}=d_{433}f_5\overline{f}_5,\ d_{442}=d_{433}f_5\overline{f}_6,\ d_{443}=d_{433}f_6\overline{f}_5,$$

$$d_{444}=d_{433}f_6\overline{f_6},\ d_{445}=d_{434}\overline{f}_5,\ d_{446}=d_{434}\overline{f_6},\ f_1=c_{53}c_{13}+c_{54}c_{16},$$

$$f_2=c_6-f_1e^{c_5},\quad f_3=c_{73}c_{13}+f_1c_{74},\quad f_4=c_8-f_3e^{c_7},\quad f_5=f_{24},\quad f_6=f_{15}+f_5f_{16},$$

$$f_7=f_8f_{18},\quad f_8=f_{25},\quad f_{28}=\varepsilon\cos\omega t\left\{f_{24}\left(\frac{e^{f_{34}}-1}{f_{34}}\right)\right\}+\left\{f_{26}\left(\frac{e^{f_{35}}-1}{f_{35}}\right)\right\},$$

$$f_{29} = \varepsilon \cos \omega t \left\{ f_{27} \left(\frac{e^{f_{36}} - 1}{f_{36}} \right) + f_{25} \left(\frac{e^{f_{37}} - 1}{f_{37}} \right) \right\}, \quad f_{30} = \frac{\lambda + \sqrt{\lambda^2 - 4c_1}}{2},$$

$$f_{31} = \frac{\lambda - \sqrt{\lambda^2 - 4c_1}}{2}, \quad f_{32} = \frac{\lambda_1 + \sqrt{\lambda_1^2 - 4c_3}}{2}, \quad f_{33} = \frac{\lambda_1 - \sqrt{\lambda_1^2 - 4c_3}}{2},$$

$$f_{34} = \frac{\lambda + \sqrt{\lambda^2 - 4\left(c_1 + \omega \tan \omega t\right)}}{2}, \quad f_{35} = \frac{\lambda - \sqrt{\lambda^2 - 4\left(c_1 + \omega \tan \omega t\right)}}{2},$$

$$f_{36} = \frac{\lambda_1 + \sqrt{\lambda_1^2 - 4\left(c_3 + \omega \tan \omega t\right)}}{2}, \quad f_{37} = \frac{\lambda_1 - \sqrt{\lambda_1^2 - 4\left(c_3 + \omega \tan \omega t\right)}}{2},$$

$$g_{13} = d_{267}, \; g_{14} = d_{266}, \; g_{15} = d_{268}, \; g_{16} = d_{265},$$

$$g_{17} = d_{335}, \; g_{18} = d_{334}, \; g_{19} = d_{336}, \; g_{20} = d_{333}.$$

References

[1] Hartmann J. (1937): *Theory of the laminar flow of an electrically conductive liquid in a homogeneous magnetic field*.– Mathematisk-fysiske Meddeleser. Det kgl. Danke Vid. Selskab, vol.15, No.6, pp.1-28.

[2] Nigam S.D. and Singh S.N. (1960): *Heat transfer by laminar flow between parallel plates under the action of transverse magnetic fields*.– Quart. J. Mech. Appl. Math.,vol.13, pp.85-97.

[3] Rudraiah N., Kumudini V. and Unno W. (1985): *Theory of nonlinear magneto convection and its application to solar convection problem.*– I. Publ. Astron. Soc., Japan, vol.37, pp.183-206.

[4] Alireza S. and Sahai V. (1990): *Heat transfer in developing magnetohydrodynamic Poiseuille flow and variable transport properties.*– Int. J. of Heat and Mass Transfer,vol.33, No.8, pp.1711-1720.

[5] Attia H.A. and Sayed Ahmed M.E. (2002): *A transient Hartmann flow with heat transfer of a non-Newtonian fluid with suction and injection, considering the Hall effect.*– J. of Plasma Physics, vol.67, No.1, pp.27-47.

[6] Cowling T.G. (1957)*: Magnetohydrodynamics*.– Interscience Publishers, Inc., New York.

[7] Sherman A. and Sutton G.W. (1961): *Magnetohydrodynamics (Evanston, Illinois)*.– p.123.

[8] Sato H. (1961): *The Hall Effect in the viscous flow of ionized gas between parallel plates under transverse magnetic field*.– J. Phys. Soc. Japan, vol.16, No.7, pp.1427-1433.

[9] Shercliff J.A. (1962): *The Theory of Electro-magnetic Flow Measurement.*– Cambridge University Press.

[10] Raju T.L. and Ramana Rao V.V. (1992): *Hall effect in the viscous flow of an ionized gas between two parallel walls under transverse magnetic field in a rotating system*.– Acta PhysicaHungarica, vol.72, No.1, pp.23-45.

[11] Ram P.C. (1995): *Effects of hall and ion-slip currents on free convective heat generating flow in a rotating fluid*.– Int. J. Energy Res., vol.19, No.5, pp.371-376.

[12] Sakhnovskii E.G. (1963): *Effects of anisotropic conductivity in Rayleigh magnetohydrodynamic problems.*– Zh. Tekhon. Fsz., vol.33, p.631.

[13] Jana R.N. and Datta N. (1977): *Hall effects on hydromagnetic flow over an impulsively started porous plate.*– Acta Mechanica, vol.28, pp.211-218.

[14] Beg O.A., Zueco J. and Takhar H.S. (2009): *Communications in nonlinear science and numerical simulation.*– vol.14, pp.1082-1097.

[15] Rama Bhargava and Meena Rani. (1984): *Magneto hydro dynamic flow and heat transfer in a channel with porous walls of different permeability*.– Indian J. Pure Appl. Math., vol.15, No.4, pp.397-408.

[16] Raju T.L. and Ramana Rao V.V. (1993): *Hall effects on temperature distribution in a rotating ionized hydromagnetic flow between parallel walls*.– Int. J. Engg. Sci., vol.31, No.7, pp.1073-1091.

[17] Ganesh S. and Krishnambal S. (2007): *Unsteady magnetohydrodynamic Stokes flow of viscous fluid between two parallel porous plates.*– Journal of Applied Sciences, vol.7, No.3, pp.374-379.

[18] Ghosh S.K., Beg O.A. and Narahari M. (2009): *Hall effects on MHD flow in a rotating system with heat transfer characteristics.*– Meccanica, vol.44, No.6, pp.741-765.

[19] Gupta A.S., Guria M. and Jana R.N.(2011): *Hall effect on the magnetohydrodynamic shear flow past an infinite porous flat plate subjected to uniform suction or blowing*.– Int.J.Nonlinear Mechanics, vol.46, No.3, pp.1057-1064.

[20] Khaled K.J. (2015) :*Influence of hall current and viscous dissipation on MHD convective heat and mass transfer in a rotating porous channel with Joule heating*.– American J. Mathematics and Statistics, vol.5, No.5, pp.272-284.

[21] Lohrasbi J. and Sahai V. (1988): *Magnetohydrodynamic heat transfer in two phase flow between parallel plates*.– Appl. Sci. Res., vol.45, pp.53-66.

[22] Malashetty M.S. and Leela V. (1991): *Proceeding of national heat transfer conference on AICHE and ASME HTD.*– p.159.

[23] Malashetty M.S. and Leela V. (1992): *Magnetohydrodynamic heat transfer in two phase flow*.– Int. J. of Engg. Sci., vol.30, pp.371-377.

[24] Chamkha A.J. (2004): *Unsteady MHD convective heat and mass transfer past a semi-infinite vertical permeable moving plate with heat absorption*.– Int. J. Engg. Sci., vol.42, pp.217-230.

[25] Sharma R.C. and Neela Rani. (1986): *Finite larmor radius and compressibility effects on thermosolutal instability of a plasma.*– Z. Naturforsch., 41a, pp.724-728.

[26] Sharma R.C. and Neela Rani. (1988): *Hall effects of thermo-solute instability of a plasma*.– Indian J. Pure Appl. Math, vol.19, No.2, pp.202-207.

[27] StamenkovićZ., NikodijevićD.D., Kocić M. and PetrovićJ.D. (2012): *MHD flow and heat transfer of two immiscible fluids with induced magnetic field.*– Thermal Science, Int. Sci. Journal, vol.16, No.2, pp.323-S336.

[28] Abdul M. (2014): *Transient magnetohydrodynamic flow of two immiscible fluids through a horizontal channel.*– Int.J.Engg.Res., vol.3, No.1, pp.13-17.

[29] Linga Raju T. (2019): *MHD heat transfer two-ionized fluids flow between two parallel plates* with *Hall currents.*– Results in Engineering, vol.4, 100043 Elsevier BV,http://doi.org/10.1016/j.rineng.2019.100043.

[30] Sivakamini L. and Govindarajan A. (2019): *Unsteady MHD flow of two immiscible fluids under chemical reaction in a horizontal channel.*– AIP conference proceedings 2112.020157, https://doi.org/10.1063/1.5112342.

[31] Abd Elmaboud Y., Abdesalam S.I., Mekheimer Kh.S. and Kambiz Vafai. (2019): *Electromagnetic flow for two-layer immiscible fluids.*–Engineering Science and Technology, an International Journal, vol.22, pp.237-248.

[32] Linga Raju T. (2021): *Electro-magneto hydrodynamic two fluid flow of ionized-gases with Hall and Rotation effects.*– Int. J. Appl. Mech., vol.26, No.4, pp.128-144. DOI: 10.2478/ijame-2021-0054.

[33] Linga Raju T. and Gowri Sankara Rao V. (2021): *Effect of Hall current on unsteady magnetohydrodynamic two-ionized fluid flow and heat transfer in a channel.*– Int. J. of Applied Mechanics and Engg., vol.26, No.2, pp.84-106.

[34] Naga Valli M., Linga Raju T. and Kameswaran P.K. (2022): *Effect of Hall currents on EMHD 2-layered plasma heat transfer flow via a channel of porous plates.*– To appear in Springer Conference Proceedings of 8th International Conference on Mathematics and Computing, (ICMC-2022) held during January6-8, 2022 at VIT, Vellore, India. Manuscript No.208.

[35] Linga Raju T. and Venkat Rao B. (2022): *Unsteady electro-magneto hydrodynamic flow and heat transfer of two ionized fluids in a rotating system with Hall currents.*– Int. J.Appl. Mech., vol.27, No.1. pp.125-145.

[36] Spitzer L. Jr. (1956): *Physics of Fully Ionized Gases.*– Interscience Publishers N. Y.

Received: November 19, 2022
Revised: April 26, 2023